Howard Hughes Medical Institute

Published as: *Nat Chem Biol*. 2016 February ; 12(2): 102–108.

Identification of cancer cytotoxic modulators of PDE3A by predictive chemogenomics

Luc de Waal[1,2], **Timothy A. Lewis**[1], **Matthew G. Rees**[1], **Aviad Tsherniak**[1], **Xiaoyun Wu**[1], **Peter S. Choi**[1,2], **Lara Gechijian**[1], **Christina Hartigan**[1], **Patrick W. Faloon**[1], **Mark J. Hickey**[1], **Nicola Tolliday**[1], **Steven A. Carr**[1], **Paul A. Clemons**[1], **Benito Munoz**[1], **Bridget K. Wagner**[1], **Alykhan F. Shamji**[1], **Angela N. Koehler**[1,3], **Monica Schenone**[1], **Alex B. Burgin**[1], **Stuart L. Schreiber**[1], **Heidi Greulich**[1,2,4,*], and **Matthew Meyerson**[1,2,5,*]

[1]The Broad Institute of Harvard and MIT, Cambridge, Massachusetts 02142, USA

[2]Department of Medical Oncology, Dana-Farber Cancer Institute, Boston, Massachusetts 02115, USA

[3]Koch Institute for Integrative Cancer Research at MIT, Cambridge, Massachusetts 02142, USA

[4]Department of Medicine, Harvard Medical School, Boston, MA 02115

[5]Department of Pathology, Harvard Medical School, Boston, MA 02115

Abstract

High cancer death rates indicate the need for new anti-cancer therapeutic agents. Approaches to discover new cancer drugs include target-based drug discovery and phenotypic screening. Here, we identified phosphodiesterase 3A modulators as cell-selective cancer cytotoxic compounds by phenotypic compound library screening and target deconvolution by predictive chemogenomics. We found that sensitivity to 6-(4-(diethylamino)-3-nitrophenyl)-5-methyl-4,5-dihydropyridazin-3(2*H*)-one, or DNMDP, across 766 cancer cell lines correlates with expression of the phosphodiesterase 3A gene, *PDE3A*. Like DNMDP, a subset of known PDE3A inhibitors kill selected cancer cells while others do not. Furthermore, *PDE3A* depletion leads to DNMDP resistance. We demonstrated that DNMDP binding to PDE3A promotes an interaction between PDE3A and Schlafen 12 (SLFN12), suggesting a neomorphic activity. Co-expression of *SLFN12* with *PDE3A* correlates with DNMDP sensitivity, while depletion of SLFN12 results in decreased

[*]Corresponding authors contributed equally to this work: ; Email: heidig@broadinstitute.org, ; Email: matthew_meyerson@dfci.harvard.edu

AUTHOR CONTRIBUTIONS

L.d.W., P.W.F., M.J.H., N.T., H.G., and M.M. designed and performed the phenotypic small molecule screen. M.G.R., A.T., A.F.S., P.A.C., A.F.S., and S.L.S. designed and performed experiments identifying *PDE3A* expression correlation with DNMDP sensitivity. L.d.W., T.A.L., L.G., B.K.W., B.M., and H.G., designed and performed experiments demonstrating physical interaction of DNMDP with PDE3A and rescue phenotype by non-cytotoxic PDE3 inhibitors. L.d.W., P.S.C., H.G., and M.M. designed and performed PDE3A protein level reduction leading to DNMDP resistance. L.d.W., X.W., C.H., S.A.C., M.S., A.B.B., H.G., and M.M. designed and performed PDE3A immunoprecipitation experiment revealing novel protein-protein interaction partners facilitated by DNMDP binding. L.d.W., X.W., M.G.R., A.T., H.G., and M.M. designed and performed experiments showing requirement of SLFN12 for DNMDP phenotype and genomic correlation with DNMDP sensitivity. L.d.W. made the figures, and L.d.W., T.A.L., H.G., and M.M. wrote the manuscript.

DNMDP sensitivity. Our results implicate PDE3A modulators as candidate cancer therapeutic agents and demonstrate the power of predictive chemogenomics in small-molecule discovery.

INTRODUCTION

Cancer kills over 550,000 people in the United States and over 8 million people world-wide each year[1]. New agents including small molecules, antibodies targeting somatic genomic alterations[2], molecules that impact tissue-specific growth requirements[3], and immunomodulatory agents[4], have been shown to benefit a subset of patients whose cancers have unique genomic mutations or other characteristics. Unfortunately, many cancer patients are still left without effective therapeutic options.

One approach to identify new anti-cancer agents is phenotypic screening to discover novel small molecules that display a strong selectivity between different cancer cell lines, followed by predictive chemogenomics to identify the cellular features associated with drug response. The cytotoxic profile of a compound can be used to identify cellular characteristics, such as gene-expression profiles and DNA copy number, that correlate with drug sensitivity[5–7]. The ability to identify the features of cancer cell lines that mediate their response to small molecules has significantly improved in recent years with the advent of automated high-throughput chemosensitivity testing of large panels of cell lines coupled with comprehensive genomic and phenotypic characterization of the cell lines[8–10]. Phenotypic observations of small-molecule sensitivity can be linked to gene expression patterns or somatic genome alterations, as in the case of *SLFN11* expression in cancer cell lines sensitive to irinotecan treatment, and an *EWS-FLI1* rearrangement in cancer cell lines sensitive to PARP inhibitors, respectively[8,10,11].

A predictive chemogenomics approach complements target-driven drug development programs, which consists of extensive *in vitro* and *in vivo* target validation, and can also be referred to as reverse chemogenomics[12]. Many U.S. Food and Drug Administration (FDA)-approved targeted therapies have been developed using this approach, among them small-molecule kinase inhibitors that target oncogenic somatic driver mutations[2]. However, the discovery and development of targeted therapies is often hampered by limited knowledge of the biological function of the target, its mechanism of action, and the available chemical matter to selectively inhibit the target[13,14].

Phenotypic screening can discover novel targets for cancer therapy whose specific molecular mechanism is often elucidated by future studies[15]. In recent years, two classes of anti-cancer drugs found by unbiased phenotypic screening efforts have been approved by the FDA: lenalidomide and pomalidomide were found to be modulators of an E3-ligase that alter the affinity of its target, leading to degradation of lineage specific transcription factors[16,17], whereas romidepsin and vorinostat were later identified as histone deacetylase (HDAC) inhibitors[2,18,19].

Tumor suppressor alterations are suitable targets for phenotypic screening as they are not directly targetable with small molecules, although synthetic lethal approaches such as olaparib treatment of *BRCA1/BRCA2* mutant cancers have proven to be effective[20]. To our

current knowledge, the *TP53* tumor suppressor gene is the most frequently mutated gene across human cancer, with somatic mutations detected in 36% of 4742 cancers subjected to whole exome sequencing[21]. Despite many attempts, no compounds have been identified that selectively kill *TP53* mutant cells by targeting a synthetic lethal interaction. We describe here a phenotypic screen developed to identify small molecules causing synthetic lethality in *TP53* mutant cancer cells, that enabled serendipitous discovery of a class of cancer-selective cytotoxic agents which act as modulators of phosphodiesterase 3A (PDE3A).

Cyclic nucleotide phosphodiesterases catalyze the hydrolysis of cyclic adenosine monophosphate (cAMP) and cyclic guanosine monophosphate (cGMP), and are important in many physiological processes[22]. Several phosphodiesterase inhibitors are approved for clinical treatment, including PDE3 inhibitors milrinone, cilostazol, and levosimendan for cardiovascular indications and inhibition of platelet coagulation, as well as the PDE3 inhibitor anagrelide for thrombocythemia. PDE5 inhibitors, *e.g.* vardenafil, are used for smooth muscle disorders including erectile dysfunction and pulmonary arterial hypertension, and the PDE4 inhibitor roflumilast reduces exacerbations from chronic obstructive pulmonary disease (COPD)[23,24]. Phosphodiesterase inhibitors act by direct enzymatic inhibition of their targets or by allosteric modulation; for example, structural analysis of PDE4 has led to the design of PDE4D and PDE4B allosteric modulators[25,26].

In this manuscript, we performed an unbiased cellular screen for cancer cytotoxic small molecules, leading to the identification of DNMDP. Genomic analysis identified a correlation between DNMDP cytotoxicity and expression of *PDE3A*. We then showed that some but not all PDE3A inhibitors have similar cytotoxic activity; that cytotoxic and non-cytotoxic inhibitors compete for PDE3A binding; and that the cytotoxic inhibitors induce a physical association between PDE3A and SLFN12. Moreover, cancer cells with high expression of both *PDE3A* and *SLFN12* are most sensitive to DNMDP, while depletion of PDE3A or SLFN12 reduces sensitivity to DNMDP. Thus our data suggest that the cancer cytotoxic phosphodiesterase modulator DNMDP may act through a gain-of-function allosteric mechanism in which it stabilizes a PDE3A-SLFN12 interaction.

RESULTS

Identification of a selective cytotoxic small molecule

To identify anti-cancer compounds with cell-selective cytotoxic activity, we performed an unbiased chemical screen in two lung adenocarcinoma cell lines, A549 and NCI-H1734, both of which harbor oncogenic *KRAS* mutations and truncating *STK11* mutations, and which are *TP53* wild type and mutant (R273L), respectively. We screened 1,924 compounds from the Molecular Libraries Small-Molecule Repository validation set (Supplementary results, Supplementary Table 1 and Supplementary Dataset 1) in the A549 and NCI-H1734 cell lines at a single concentration of 10 μM in 384-well format in duplicate. As a proxy for cellular viability, we measured ATP content after 48 hours of compound treatment.

Three compounds showed a selective reduction in cell viability for the NCI-H1734 cell line compared to the A549 cell line, with an approximately 50% reduction in the NCI-H1734 cell line, which is > 4 median absolute deviations from the median in the negative direction,

compared to a minimal change of < 1 median absolute deviations from the median in the A549 cell line (Fig. 1a). Retesting the three compounds in a dose–response analysis validated that one compound, 6-(4-(diethylamino)-3-nitrophenyl)-5-methyl-4,5-dihydropyridazin-3(2*H*)-one, or DNMDP (**1**), was specifically toxic to the NCI-H1734 cell line (Fig. 1).

Testing of additional cell lines with DNMDP showed clear cell-selective cytotoxicity. For example, six illustrative cell lines showed an EC_{50} between 10 and 100 nM for two additional lung adenocarcinoma cell lines, NCI-H1563 and NCI-H2122, and for HeLa cervical carcinoma cells, but an EC_{50} greater than 1 μM for A549, MCF7, and PC3 cells (Fig. 1b). HeLa cells undergo apoptosis upon DNMDP treatment, indicated by caspase activity detected by a caspase-sensitive luciferase assay and by poly ADP ribose polymerase (PARP) cleavage (Supplementary Fig. 2a and 2b). To further characterize cellular sensitivity to DNMDP further, we treated 766 genomically characterized cancer cell lines with DMNDP for 72 hours at concentrations ranging from 66.4 μM to 2 nM in 2-fold dilution increments. Of these, 22 cell lines were sensitive to DNMDP with a robust Z-score lower than -4, which represented multiple lineages including multiple melanoma cell lines, amongst others (Supplementary Dataset 2).

Next, we separated the DNMDP enantiomers by chiral super-critical fluid (SCF) chromatography. One enantiomer was 500-fold more potent in HeLa cells than the other (Fig. 1c and 1d). The (*R*)-enantiomer was synthesized from optically pure starting materials (Supplementary Note). This synthesized enantiomer had similar activity to the more potent separated material and was identical by chiral SCF chromatography, confirming stereochemistry of the active enantiomer (Supplementary Note). We also synthesized two (*R*)-*des*-nitro analogues of DNMDP, DNMDP-2 (**2**) and DNMDP-3 (**3**), both of which tested similarly to (*R*)-DNMDP (**1**) (Supplementary Note).

Identification of PDE3A as a putative target of DNMDP

Given the potent cell-selective growth inhibition by DNMDP, we sought to understand its mechanism of action. To determine the molecular target of DNMDP, we performed chemogenomic analysis of the 766 tested cell lines, previously characterized for mutations, copy number, and gene expression features as part of the Cancer Cell Line Encyclopedia (CCLE)[8], to look for correlations between these genomic features and DNMDP sensitivity. Analysis of Pearson correlations between DNMDP sensitivity and expression of individual genes across the cell line set showed a strong correlation with expression of the *PDE3A* gene, encoding for phosphodiesterase 3A (Fig. 2a). The Pearson correlation between DNMDP sensitivity and *PDE3A* expression is 0.42 and a Z-score of approximately 8.5 (Supplementary Fig. 3). As shown below, expression of other factors also influence sensitivity, and it is possible that some errors are introduced due to the high-throughput nature of the cell line sensitivity characterization, as manual validation for all 766 cell lines was not logistically feasible. Mutation and copy number features, in contrast, did not correlate with DNMDP sensitivity. Conversely, of 480 compounds tested, DNMDP sensitivity is the closest correlate of *PDE3A* expression (Fig. 2b), indicating that cancer cell lines with high *PDE3A* expression are more distinctly sensitive to DNMDP than to any other

tested compound. In contrast to the motivation of our initial screen, there was no correlation between *TP53* mutation, or other measures of p53 function, and DNMDP sensitivity.

Given these results and the clear structural similarity of DNMDP to known PDE3 inhibitors, *e.g.*, levosimendan and siguazodan (Supplementary Fig. 4), we performed biochemical analysis of DNMDP against 19 phosphodiesterases representing 11 PDE families. At a concentration of 100 nM, DNMDP specifically inhibited both PDE3A and PDE3B, weakly inhibited PDE10, and had little or no detectable effect on other phosphodiesterases (Supplementary Table 2).

Because of the cellular correlation between *PDE3A* expression and DNMDP sensitivity, the *in vitro* inhibition of PDE3A and PDE3B by DNMDP, and the structural similarity of DNMDP to known PDE3 inhibitors, we analyzed whether all PDE3 inhibitors would exhibit a similar cytotoxic profile to DNMDP. Surprisingly, there was almost no correlation between IC_{50} for *in vitro* enzymatic PDE3A inhibition and HeLa cell cytotoxicity across a series of tested compounds (Fig. 2c and Supplementary Fig. 5). Indeed, the potent PDE3 inhibitor trequinsin (PDE3 IC_{50} = 0.25 nM[27]) did not affect HeLa cell viability in any detectable way. Despite their differential effects on HeLa cell viability, the non-cytotoxic PDE3 inhibitor trequinsin and the potent cytotoxic compound DNMDP had similar effects on intracellular cAMP levels in forskolin-treated HeLa cells (Supplementary Fig. 6). This result suggests that inhibition of the cAMP and cGMP hydrolysis functions of PDE3A is not sufficient for the cytotoxic activity of DNMDP.

Target validation of PDE3A

The complex relationship between PDE3A inhibition and cell killing, in which DNMDP and some PDE3 inhibitors kill HeLa and other DNMDP-sensitive cells, whereas others PDE3 inhibitors do not affect cell viability, suggested several possible interpretations including: 1) the cytotoxic activity might be PDE3-independent and due to action on a different protein though screening 234 kinases found no kinase inhibition by 10 μM DNMDP (Supplementary Table 3); 2) cytotoxic and non-cytotoxic PDE3 inhibitors might bind to different sites within the protein and exert distinct activities; or 3) the cytotoxic and non-cytotoxic PDE3 inhibitors might bind to the PDE3 active sites but have different effects on the conformation and activity of the protein. This third possibility may be unexpected, but allosteric modulators of PDE4 have been shown to bind the PDE4 active site and interact with upstream (UCR2), and downstream (CR3) regulatory domains and thereby stabilize specific inactive conformations[25]. Most notably, PDE4 competitive inhibitors and PDE4 allosteric modulators with similar IC_{50}s for cAMP hydrolysis *in vitro* exhibit different cellular activities and safety profiles in animal studies[25]. To evaluate whether PDE inhibitors or other small molecules compete with DNMDP, we screened the Pharmakon 1600 collection of 1600 bioactive compounds (http://www.msdiscovery.com/pharma.html) to identify compounds that were able to rescue cell death induced by DNMDP (Supplementary Dataset 3). We treated HeLa cells with 30 nM DNMDP (the EC_{70} concentration) and 20 μM of each bioactive compound for 48 hours, and assessed cell viability by ATP consumption as described earlier. The five most potent compounds that rescued cell death induced by

DNMDP were all PDE inhibitors, and the three most potent compounds, levosimendan, milrinone, and cilostazol, were all selective PDE3 inhibitors (Fig. 3a).

In follow-up experiments, we confirmed that cilostamide, levosimendan, milrinone, and several other non-cytotoxic selective PDE3 inhibitors were able to rescue DNMDP cytotoxicity in a dose-dependent manner (Fig. 3b). The most potent DNMDP competitor was trequinsin, with an "RC_{50}" (the concentration at which it achieved 50% rescue) of < 1 nM; in contrast, PDE5 inhibitors such as sildenafil and vardenafil, as well as the pan-PDE inhibitors idubilast and dipyridamole, were not effective competitors up to 10 μM concentrations in this assay (Fig. 3b). This suggests that non-cytotoxic PDE3 inhibitors and DNMDP compete for binding to the same molecular target that is mediating the cytotoxic phenotype.

To identify the molecular target of DNMDP, we performed an affinity purification using an (*R*)-*des*-nitro-DNMDP solid-phase tethered linker analogue, DNMDP-2L (**4**), (Supplementary Fig. 7a) incubated with HeLa cell lysate. This linker analogue has the same DNMDP cytotoxicity rescue phenotype as non-cytotoxic PDE3 inhibitors described above (Supplementary Fig. 7b), suggesting that it too binds to the same molecular target. We competed for the molecular target by adding either an excess of trequinsin or separate enantiomers of DNMDP, where only the (*R*)-enantiomer is cytotoxic. Immunoblotting for PDE3A of the affinity purified material showed that PDE3A indeed binds to the linker analogue. Binding of PDE3A to the linker analogue is blocked by both trequinsin and (*R*)-DNMDP, but not by the non-cytotoxic enantiomer (*S*)-DNMDP (**5**) (Fig. 3c). Thus both trequinsin and (*R*)-DNMDP prevent the binding of PDE3A to the tethered DNMDP analogue, and we conclude that both molecules bind PDE3A directly.

Based on the observations that DNMDP-sensitive cells express high levels of PDE3A, and that DNMDP competes with non-cytotoxic inhibitors for PDE3A binding, we hypothesized that DNMDP mediates its cytotoxic phenotype through the interaction with PDE3A and that PDE3A abundance is a direct cellular determinant of DNMDP sensitivity. To validate this hypothesis, we tested the effect of reducing levels of PDE3A on the response to DNMDP. A clustered regularly interspaced short palindromic (CRISPR)-associated CAS9 enzyme that was targeted with three guide RNAs (sgRNA) targeting three different sites in the *PDE3A* locus lead to complete loss of PDE3A expression[28]. sgRNA2 and sgRNA3 almost completely reduced PDE3A protein levels, whereas sgRNA1 only had a moderate effect on PDE3A expression (Fig. 4a). Strikingly, both sgRNA2 and sgRNA3 led to significant rescue of toxicity by DNMDP (Fig. 4b). In an independent approach using an siRNA smart-pool containing four different siRNAs targeting *PDE3A*, we reduced PDE3A expression in HeLa cell line with a maximum efficiency of 70% between 24 and 72 hours after transfection. HeLa cells treated with siPDE3A had a higher EC_{50} to a DNMDP analog compared to the control siRNA condition (Supplementary Fig. 8). We conclude that DNMDP cytotoxicity requires PDE3A, and that DNMDP likely modulates the function of PDE3A.

Determining the mechanism of action of DNMDP

The dependence of DNMDP cytotoxicity on PDE3A protein abundance suggests a possible mechanism similar to that recently observed for lenalidomide, which acts by a neomorphic

or hypermorphic mechanism by stabilizing an interaction between cereblon and IKZF1 and IKZF3[16,17]. In addition, PDE4 allosteric modulators, but not competitive inhibitors, have been shown to bind and stabilize a “closed” protein conformation that has independently been shown to uniquely bind the PDE4-partner protein DISC1[29]. We characterized the protein complexes in which PDE3A resides under normal conditions, and how these complexes change when PDE3A is bound to DNMDP or the non-cytotoxic PDE3 inhibitor trequinsin. We immunoprecipitated PDE3A and interacting proteins from HeLa cells in the presence of DNMDP or trequinsin followed by labeling with isobaric stable isotope tags for relative abundance and quantitation by mass spectrometry (iTRAQ/MS) (Supplementary Fig. 9). PDE3A immunoprecipitates from HeLa cells showed enrichment for multiple protein phosphatase subunits including protein phosphatase 2 subunits (PPP2CA, PPP2R1A, PPP2R1B, PPP2R2A, PPP2R2D), calcineurin (PPP3R1, PPP3CA)[30], 14-3-3 (YWHAB, YWHAQ, YWHAG, YWHAZ)[31], and tubulin (TUBA1C, TUBA1B) family members (Fig. 5a and Supplementary Fig. 10a and Supplementary Dataset 4). In addition, we found that PDE3A and PDE3B reside in the same protein complex, which has been previously reported[32].

Binding of DNMDP altered the composition of interacting proteins that were co-immunoprecipitated with PDE3A. Specifically enriched proteins in the PDE3A immunoprecipitates after treatment with DNMDP included Sirtuin 7 (SIRT7) and Schlafen 12 (SLFN12) (Fig. 5b and Supplementary Fig. 10b and Supplementary Dataset 4). These proteins specifically interacted with PDE3A in the presence of DNMDP, and not observed in the trequinsin treated control, whereas a known PDE3B interactor, ABHD15[33], was enriched in the immunoprecipitate from trequinsin-treated cells (Fig. 5b and Supplementary Fig. 10c and Supplementary Dataset 4). We validated the interaction promoted by DNMDP between PDE3A and both SIRT7 and SLFN12 with affinity reagents. Immunoprecipitation of endogenous PDE3A in HeLa cells treated with DNMDP, but not DMSO or trequinsin, enhanced complex formation of ectopically expressed V5-tagged SIRT7 and SLFN12 with PDE3A, as evidenced by co-immunoprecipitation (Fig 5c).

The enhanced interaction of PDE3A with SIRT7 and SLFN12 suggests the possibility that one or more of these interacting proteins may contribute to DNMDP sensitivity. *SIRT7* mRNA expression is relatively constant among all cells tested, but the co-expression of *SLFN12* and *PDE3A* mRNA showed a strong correlation with DNMDP sensitivity; almost all DNMDP-sensitive cell lines express high levels of *SLFN12* (Fig. 6a). Strikingly, almost half of sensitive cell lines expressing high levels *SLFN12* and *PDE3A* were melanoma cell lines (Fig. 6b). *SLFN12* expression alone was also one of the top genes correlating with sensitivity to DNMDP, corroborating the hypothesis that SLFN12 could be functionally involved in DNMDP-induced cytotoxicity (Supplementary Fig. 11a). Moreover, when correcting for *PDE3A* expression, *SLFN12* expression is the top correlating gene with DNMDP sensitivity (Supplementary Fig. 11b). To assess whether SLFN12 is required for the cytotoxic phenotype of DMNDP, we reduced *SLFN12* mRNA expression by 60% by knockdown with two shRNAs in HeLa cells (Fig. 6c). Similar to reduction in PDE3A expression, reduction of SLFN12 expression did not result in cytotoxicity, and in fact decreased sensitivity to DNMDP (Fig. 6d). These results show that SLFN12, like PDE3A, is required for the cytotoxic phenotype of DMNDP. Characterization of normal expression of

SLFN12 and *PDE3A* by the GTEX consortium[34] shows low expression of *SLFN12* in normal tissues, while high co-expression of both *PDE3A* and *SLFN12* is rarely observed (Supplementary table 4). This could suggest that on-target toxicity of DNMDP and related compounds may be potentially limited.

Using predictive chemogenomics, we have discovered a class of compounds, exemplified by DNMDP, that target a novel cancer dependency by small-molecule modulation of PDE3A. These compounds bind PDE3A in a mutually exclusive manner with non-cytotoxic PDE3 inhibitors and exert a neomorphic or hypermorphic effect on the function of PDE3A, leading to a change in its protein-protein interactions. One protein-interaction partner, SLFN12, is highly expressed in DNMDP-sensitive cell lines, suggesting a functional role in the pathway through which the cytotoxic signal is relayed. As a result, DNMDP is both selective and potent across a large panel of cancer cell lines.

DISCUSSION

Here, we have identified a novel cytotoxic compound exhibiting great selectivity and low nanomolar potency against cancer cell lines across multiple lineages. Using gene-expression correlates for predictive chemogenomics, we identified PDE3A as the putative target of this small molecule, DNMDP. Single gene or multi-gene expression correlations can help elucidate the mechanism of action and relevant signaling pathways of small molecules. We identified a novel biochemical target for cancer treatment that is unlikely to have been found by traditional target identification approaches such as loss-of-function screens or genomic analysis of patient tumor samples.

PDE3A expression is highest in the cardiovascular system, platelets, kidney, and oocytes, and the clinical PDE3 inhibitor cilostazol has been developed to treat intermittent claudication, as PDE3A inhibition in platelets impairs activation and platelet coagulation[35,36]. Other PDE3 inhibitors, such as milrinone, amrinone, and levosimendan, are indicated to treat congestive heart failure, where the combination of vasodilation and elevated cardiac cAMP levels increases cardiac contractility[37]. None of these inhibitors were able to replicate the cytotoxic phenotype of DNMDP, suggesting that cyclic nucleotide hydrolysis is not sufficient to induce cell death in DNMDP-sensitive cell lines.

Interestingly however, other PDE3 inhibitors such as zardaverine, anagrelide, and quazinone have been reported previously to have cell cytotoxic characteristics in a select number of cancer cell lines[38,39], with anagrelide uniquely inhibiting megakaryocyte differentiation, resulting in apoptosis. However, other PDE3 inhibitors tested did not have this activity[40,41]. We hypothesize that the reported effects of zardaverine on cell viability and anagrelide on megakaryocyte differentiation are mediated through modulation of PDE3A function in a manner similar to what we describe in this study.

Many PDE3 inhibitors act as competitive inhibitors, occupying the catalytic cAMP and cGMP binding site[42,43]. In addition, zardaverine has been co-crystalized in a complex with PDE4D, where it occupies the cAMP-binding site, and is predicted to bind PDE3B in a similar manner[44]. Given the structural similarity of DNMDP to zardaverine, the binding

mode of DNMDP may be similar. However, allosteric modulation of phosphodiesterases has been described previously for PDE4, where small molecules bind the active site and simultaneously interact with nearby regulatory domains. As a result, allosteric modulators stabilize a protein conformation that has been shown to differentially bind different PDE4 partner proteins[25].

The study of proteins associated with PDE3A may illuminate both its normal function and the way in which PDE3A modulators such as DNMDP kill cancer cells. PDE3A interacts with protein phosphatase 2 subunits, which are implicated in oncogenic viral transformation and are mutated in human cancers[45–47], suggesting a role for PDE3A in cancer cell signaling. Even though these interactions are not induced by DNMDP binding, the importance of the protein phosphatases in cancer biology would warrant further research.

The interaction between PDE3A and SLFN12, promoted by DNMDP binding to PDE3A, the correlation between sensitivity to DNMDP with *SLFN12* expression, and the requirement of SLFN12 for the DNMDP phenotype strongly suggests that we need to understand the functional impact of the PDE3A-SLFN12 interaction. However, little is known at this time about the functional role of SLFN12 in human physiology and cancer biology. Additional studies into the function of SLFN12 and its interaction with PDE3A could elucidate the mechanism of DNMDP cytotoxicity.

Two observations suggest that DNMDP does not simply act to inhibit PDE3A enzymatic function: 1) DNMDP-sensitive cancer cell lines do not depend on PDE3A expression for survival, but rather PDE3A knock-down leads to DNMDP resistance; and 2) DNMDP induces or enhances protein-protein interactions upon binding to PDE3A. This is similar to the activity of lenalidomide, which modulates a specific protein-protein interaction between the cereblon ubiquitin ligase and Ikaros transcription factors, which are subsequently targeted for degradation[16,17]. By analogy, DNMDP may directly stabilize a PDE3A-SLFN12 interaction, or DNMDP could allosterically stabilize a PDE3A conformation that binds SLFN12, resulting in a neomorphic or hypermorphic phenotype. Further characterization of the neomorphic phenotype induced by DNMDP might facilitate synthesis of small molecules that dissociate the anticancer phenotype from PDE3A cyclic nucleotide hydrolysis. Toxicity profiles of such small molecules should differ from PDE3 inhibitors prescribed for cardiovascular indications.

This study has uncovered a previously unknown role for PDE3A in cancer maintenance, in which its function can be modified by a subset of PDE3 inhibitors, resulting in toxicity to cancer cell lines expressing elevated levels of PDE3A and SLFN12. Our data suggest that DNMDP and its analogs modulate PDE3A activity, leading to apoptosis in sensitive cell lines. Our observations are comparable with other reports of allosteric modulation of phosphodiesterases[25], suggesting that DNMDP and analogues may have similar effects on PDE3A. Further study is required to elucidate the exact mechanism of cell-selective cytotoxicity induced by neomorphic modulation of PDE3A and SLFN12.

ONLINE METHODS

Compound library screening in NCI-H1734 and A549 cell lines

1500 NCI-H1734 or 1000 A549 cells were plated in a 384-well plate in 40 μl of RPMI supplemented with 10% Fetal Bovine Serum and 1% Pen/Strep. 24 hours after plating, a compound-library of 1924 small molecules was added at a concentration of 10 μM. Staurosporine was used a positive control for cytotoxicity at a concentration of 10 μM, and DMSO was used a negative control at a concentration of 1%. All compounds were incubated for 48 hours with indicated small molecules. After 48 hours, 384-well plates were removed from the incubator and allowed to cool to room temperature for 20 minutes. Cell viability was assessed by adding 40 μl of a 25% CellTiter-Glo (Promega) in PBS with a Thermo Combi or multichannel-pipette and incubated for 10 min. The luminescence signal was read using a Perkin-Elmer EnVision. Viability percentage was calculated by normalizing to DMSO controls. All cell lines were acquired from ATCC.

Compound sensitivity testing in cell lines

1000 HeLa (DMEM), 1000 A549 (RPMI), 500 MCF-7 (DMEM), 4000 PC3 (F12-K), 1000 NCI-H2122 (RPMI) or 1500 NCI-H1563 (RPMI) cells were plated in a 384-well plate in 40 μl of corresponding growth media supplemented with 10% Fetal Bovine Serum. 24 hours after plating, indicated compounds were added at indicated concentrations and incubated for 48 hours. Cell viability was assessed as described in *Compound library screening in NCI-H1734 and A549 cell lines*. All cell lines were acquired from ATCC.

Caspase activity in HeLa cells

1000 HeLa cells were plated in 384-well plate in 40 μl of corresponding growth media supplemented with 10% Fetal Bovine Serum. 24 hours after plating, indicated compounds were added at indicated concentrations and incubated for 48 hours. Caspase-Glo from Promega was added according to the manufacturers recommendations and luminescence was determined as described in *Compound library screening in NCI-H1734 and A549 cell lines*.

Large-scale cell-line viability measurements

We measured the sensitivity of 777 cancer cell lines (CCLs) drawn from 23 different lineages to DNMDP. Cancer cell lines are part of the Cancer Cell Line Encyclopedia and have their identities confirmed through SNP-arrays and somatic DNA alterations. Each cell line was plated in its preferred media in white opaque 1536-plates at a density of 500 cells/well. After incubating overnight, compound 1b was added by acoustic transfer at 16 concentrations ranging from 66.4 μM – 2 nM in 2-fold steps in duplicate (Labcyte Echo 555, Labcyte Inc., Sunnyvale, CA). After 72 h treatment, cellular ATP levels were measured as a surrogate for viability (CellTiterGlo®, Promega Corporation, Madison, WI) according to manufacturer's protocols using a ViewLux Microplate Imager (PerkinElmer, Waltham, MA) and normalized to background (media-only) and vehicle (DMSO)-treated control wells.

Concentration response curves were fit using nonlinear fits to 2- or 3-parameter sigmoid functions through all 16 concentrations with the low-concentration asymptote set to the DMSO-normalized value, and an optimal 8-point dose curve spanning the range of

compound-sensitivity was identified. The area under the 8-point dose curve (AUC) was computed by numeric integration as a metric for sensitivity for further analysis. Similar sensitivity measurements have been obtained for a collection of 480 other compounds, enabling analyses that identify cell lines responding uniquely to DNMDP (see http://www.broadinstitute.org/ctrp for complete list of compounds).

Correlation of sensitivity measurements with basal gene expression

Gene-centric robust multichip average (RMA)-normalized basal mRNA gene expression data measured on the Affymetrix GeneChip Human Genome U133 Plus 2.0 Array were downloaded from the Cancer Cell Line Encyclopedia (http://www.broadinstitute.org/ccle). Pearson correlation coefficients were calculated between gene expression (18,988 transcripts) and AUCs across 760 overlapping CCLs. For comparisons across small molecules exposed to differing numbers of CCLs, correlation coefficients were transformed using Fisher's transformation.

Bioactives screen to rescue DNMDP induced cytotoxicity

1000 HeLa cells were plated in a 384-well plate in 40 µl of DMEM supplemented with 10% Fetal Bovine Serum and 1% Pen/Strep. 24 hours after plating, a compound-library of 1600 bioactive molecules (Pharmakon) was added at a concentration of 20 µM. In parallel to bioactive compound incubation, DNMDP was added to a final concentration of 30 nM and incubated for 48 hours. Cell viability was assessed as described in *Compound library screening in NCI-H1734 and A549 cell lines*.

Linker-affinity purification of molecular target of DNMDP and immunoblotting

HeLa cells were washed with ice-cold PBS before lysed with NP-40 lysis buffer (150 mM NaCl, 10% glycerol, 50 mM Tris-Cl pH 8.0, 50 mM $MgCl_2$, 1% NP-40) supplemented with EDTA-free protease inhibitors (Roche) and phosphatase inhibitor mixtures I and II (Calbiochem). Cell lysates were incubated on ice for at least 2 minutes and subsequently centrifuged for 10 minutes at 4° C at 15,700 × g after which the supernatant was quantified using BCA protein assay kit (Pierce). 200 µg total HeLa cell lysate was incubated with 3 µl Affi-Gel 102 resin (BioRad) coupled to affinity linker DNMDP-2L in a total volume of 400 µl for four hours. Prior to incubation, indicated compounds were added to affinity purifications at a final concentration of 10 µM. Samples were washed three times with lysis buffer containing corresponding compound concentrations of 10 µM. Proteins bound to Affi-Gel 102 resin were reduced, denatured, and separated using Tris-Glycine gels (Novex) and transferred to nitrocellulose membranes using the iBlot transfer system (Novex). Membranes were incubated overnight at 4° C with primary antibodies against PDE3A (1:1000, Bethyl #A302-740). Incubation with secondary antibodies (1:20,000, LI-COR Biosciences) for two hours at room temperature and subsequent detection (Odyssey Imaging System, LI-COR Biosciences) were performed according to manufacturers recommendations.

PARP-cleavage immunoblotting

HeLa cells were treated with indicated concentration of DNMDP and staurosporine for 36 hours. HeLa cells were lysed and processed as described in *Linker-affinity purification of*

molecular target of DNMDP and immunoblotting. Membranes were incubated with an antibody against PARP (1:1000, Cell Signaling #9532) and actin (1:20,000, Cell Signaling #3700) and subsequently imaged as described in *Linker-affinity purification of molecular target of DNMDP and immunoblotting*.

Targeting PDE3A locus using CRISPR

CRISPR target sites were identified using the MIT CRISPR Design Tool (http://crispr.mit.edu). For cloning of sgRNAs, forward and reverse oligos were annealed, phosphorylated and ligated into BsmBI-digested pXPR_BRD001. Oligo sequences are listed in Supplementary Table 5. To produce lentivirus, 293T cells were co-transfected with pXPR_BRD001, psPAX2 and pMD2.G using calcium phosphate. Infected HeLa cells were selected with 2ug/ml of puromycin.

Reduction of PDE3A expression using siRNA

HeLa cells were plated in 96-well plates and transfected after 24 hours with PDE3A and Non-Targeting siRNA smartpools (On Target Plus, Thermo Scientific) according to the manufacturers recommendations. HeLa cell lysate was obtained 24 hours and 72 hours after transfection and immunoblotted for PDE3A and Actin (1:20,000, Cell Signaling) as described in *Linker-affinity purification of molecular target of DNMDP and immunoblotting*. HeLa cells were treated for 48 hours with indicated concentrations of Compound 3 (supplementary figure 2). Cell viability was assessed as described in *Compound library screening in NCI-H1734 and A549 cell lines*.

Measuring cellular cAMP concentrations in HeLa cells

5000 HeLa cells were plated in 96-well plates. 24 hours after plating, HeLa cells were incubated for one hour with indicated compounds at indicated concentrations. cAMP levels were determined with the cAMP-Glo assay (Promega) according to the manufacturers recommendations. Cellular concentrations of cAMP were determined by normalizing to a standard curve generated according to the manufacturers recommendations.

Extended Proteomics Methods for PDE3A-protein interaction studies

Immunoprecipitation of PDE3A in HeLa cells—HeLa cells were treated for four hours prior to lysis with 10 μM of indicated compounds: DMSO, DNMDP and trequinsin. HeLa cells were lysed with ModRipa lysis buffer (1%NP-40: 50 mM Tris-HCl, pH 7.8, 150 mM NaCl, 0.1% sodium deoxycholate, 1 mM EDTA) supplemented with protease and phosphatase inhibitors as decribed in *Linker-affinity purification of molecular target of DNMDP and immunoblotting*, and indicated compounds as described above to a final concentration of 10 μM. 13 mg of HeLa total cell lysate was incubated with 0.5% PDE3A antibody (Bethyl) and incubated overnight. Blocking peptide (Bethyl) against the PDE3A antibody was added simultaneously with the PDE3A antibody in the corresponding condition. Total cell lysate and antibody mixture was then incubated with 10 μl Protein A Plus Agarose (Fisher Scientific) for 30 minutes at 4° C. Protein A Plus Agarose was then washed two times with lysis buffer containing indicated compounds at a concentration of 10

µM. Finally, Protein A Plus Agarose was washed once with lysis buffer containing no NP-40 and indicated compounds at a concentration of 10 µM.

On-bead digest—The beads from immunopurification were washed once with IP lysis buffer, then three times with PBS, the three different lysates of each replicate were resuspended in 90 µl digestion buffer (2M Urea, 50 mM Tris HCl), 2 ug of sequencing grade trypsin added, 1 hour shaking at 700rpm. The supernatant was removed and placed in a fresh tube. The beads were then washed twice with 50 µl digestion buffer and combined with the supernatant. The combined supernatants were reduced (2 µl 500 mM DTT, 30 minutes, RT), alkylated (4 µl 500 mM IAA, 45 minutes, dark) and a longer overnight digestion performed: 2 ug (4 µl) trypsin, shake o/n, The samples were then quenched with 20 µl 10% FA and desalted on 10 mg SepPak columns.

iTRAQ labeling of peptides and strong cation exchange (scx) fractionation—Desalted peptides were labeled according to the manufacturer's instructions with four different isobaric iTRAQ reagents ranging from 114 to 117 Da, as described in Supplementary Table 6 (AB Sciex, Foster City, CA). Peptides were dissolved in 30 µl of 0.5 M TEAB pH 8.5 solution and labeling reagent was added in 70 µl of ethanol. After 1 h incubation the reaction was stopped with 50 mM Tris/HCl pH 7.5. Differentially labeled peptides were mixed and subsequently desalted on 10 mg SepPak columns. SCX fractionation of the differentially labelled and combined peptides was done as described in Rappsilber et al[51], with 6 pH steps (buffers- all contain 25% acetonitrile) as below:

1: ammonium acetate 50 mM pH 4.5,

2: ammonium acetate 50 mM pH 5.5,

3: ammonium acetate 50 mM pH 6.5,

4: ammonium bicarbonate 50 mM pH 8,

5: ammonium hydroxide 0.1% pH 9,

6: ammonium hydroxide 0.1% pH 11.

Empore SCX disk used to make StageTips as described in the paper.

MS analysis

Reconstituted peptides were separated on an online nanoflow EASY-nLC 1000 UHPLC system (Thermo Fisher Scientific) and analyzed on a benchtop Orbitrap Q Exactive mass spectrometer (Thermo Fisher Scientific). The peptide samples were injected onto a capillary column (Picofrit with 10 µm tip opening / 75 µm diameter, New Objective, PF360-75-10-N-5) packed in-house with 20 cm C18 silica material (1.9 µm ReproSil-Pur C18-AQ medium, Dr. Maisch GmbH, r119.aq). The UHPLC setup was connected with a custom-fit microadapting tee (360 µm, IDEX Health & Science, UH-753), and capillary columns were heated to 50 °C in column heater sleeves (Phoenix-ST) to reduce backpressure during UHPLC separation. Injected peptides were separated at a flow rate of 200 nL/min with a linear 80 min gradient from 100% solvent A (3% acetonitrile, 0.1% formic acid) to 30% solvent B (90% acetonitrile, 0.1% formic acid), followed by a linear 6 min gradient from

30% solvent B to 90% solvent B. Each sample was run for 120 min, including sample loading and column equilibration times. The Q Exactive instrument was operated in the data-dependent mode acquiring HCD MS/MS scans (R=17,500) after each MS1 scan (R=70,000) on the 12 top most abundant ions using an MS1 ion target of 3×10^6 ions and an MS2 target of 5×10^4 ions. The maximum ion time utilized for the MS/MS scans was 120 ms; the HCD-normalized collision energy was set to 27; the dynamic exclusion time was set to 20s, and the peptide match and isotope exclusion functions were enabled.

Quantification and identification of peptides and proteins

All mass spectra were processed using the Spectrum Mill software package v4.1 beta (Agilent Technologies), which includes modules developed by us for iTRAQ -based quantification. Precursor ion quantification was done using extracted ion chromatograms (XIC's) for each precursor ion. The peak area for the XIC of each precursor ion subjected to MS/MS was calculated automatically by the Spectrum Mill software in the intervening high-resolution MS1 scans of the LC-MS/MS runs using narrow windows around each individual member of the isotope cluster. Peak widths in both the time and *m/z* domains were dynamically determined based on MS scan resolution, precursor charge and *m/z*, subject to quality metrics on the relative distribution of the peaks in the isotope cluster vs theoretical. Similar MS/MS spectra acquired on the same precursor m/z in the same dissociation mode within +/− 60 sec were merged. MS/MS spectra with precursor charge >7 and poor quality MS/MS spectra, which failed the quality filter by not having a sequence tag length > 1 (i.e., minimum of 3 masses separated by the in-chain mass of an amino acid) were excluded from searching.

For peptide identification MS/MS spectra were searched against human Uniprot database to which a set of common laboratory contaminant proteins was appended. Search parameters included: ESI-QEXACTIVE-HCD scoring parameters, trypsin enzyme specificity with a maximum of two missed cleavages, 40% minimum matched peak intensity, +/− 20 ppm precursor mass tolerance, +/− 20 ppm product mass tolerance, and carbamidomethylation of cysteines and iTRAQ labeling of lysines and peptide n-termini as fixed modifications. Allowed variable modifications were oxidation of methionine, N-terminal acetylation, Pyroglutamic acid (N-termQ),Deamidated (N),Pyro Carbamidomethyl Cys (N-termC),with a precursor MH+ shift range of −18 to 64 Da. Identities interpreted for individual spectra were automatically designated as valid by optimizing score and delta rank1-rank2 score thresholds separately for each precursor charge state in each LC-MS/MS while allowing a maximum target-decoy-based false-discovery rate (FDR) of 1.0% at the spectrum level.

In calculating scores at the protein level and reporting the identified proteins, redundancy is addressed in the following manner: the protein score is the sum of the scores of distinct peptides. A distinct peptide is the single highest scoring instance of a peptide detected through an MS/MS spectrum. MS/MS spectra for a particular peptide may have been recorded multiple times, (i.e. as different precursor charge states, isolated from adjacent SCX fractions, modified by oxidation of Met) but are still counted as a single distinct peptide. When a peptide sequence >8 residues long is contained in multiple protein entries in the sequence database, the proteins are grouped together and the highest scoring one and its

accession number are reported. In some cases when the protein sequences are grouped in this manner there are distinct peptides which uniquely represent a lower scoring member of the group (isoforms or family members). Each of these instances spawns a subgroup and multiple subgroups are reported and counted towards the total number of proteins.iTRAQ ratios were obtained from the protein-comparisons export table in Spectrum Mill. To obtain iTRAQ protein ratios the median was calculated over all distinct peptides assigned to a protein subgroup in each replicate. To assign interacting proteins we used the Limma package in the R environment to calculate moderated *t*-test *p*, as described previously and added Blandt-Altman testing to filter out proteins for which the CI for reproducibility was below 95%[52].

Validation of DNMDP-induced PDE3A protein interactions using immunoprecipitation and immunoblotting

HeLa cells were transfected with ORF overexpression constructs expressing V5-tagged SIRT7, V5-tagged SLFN12, or V5-tagged GFP. ORF expression constructs were obtained from the TRC (clone IDs: TRCN0000468231, TRCN0000476272, ccsbBroad304_99997). At 72 hours post transfection, cells were treated with 10 μM DNMDP or trequinsin for 4 hours followed by lysis using the ModRipa lysis buffer and immunoprecipitation of PDE3A. For each condition, 2 mg total protein lysate was incubated with 1 μg of anti-PDE3A antibody at 4° C overnight, after which 7.5 μl each of Protein A- and Protein G- Dynabeads (Life Technologies 10001D and 10003D) were added and incubated for another 1 hour. Beads were washed and bound proteins were eluted with 30 μl of LDS PAGE gel loading buffer. Input (~60 μg total protein lysate) and IP products were resolved on 4-12% Tris-Glycine PAGE gels and immunoblotted with an anti-V5 antibody (Life Technologies R96205, 1:5000), the Bethyl anti-PDE3A antibody (1:1000), and secondary antibodies from LiCOR Biosciences (Cat.# 926-32210 and 926068021, each at 1:10,000). Blots were washed and imaged using a LiCOR Odyssey infrared imager.

Knockdown of *SLFN12* expression using shRNA and testing for drug sensitivity

Constructs expressing shRNAs targeting *SLFN12*, or the control vector, were packaged into lentiviruses and delivered into HeLa cells by viral transduction. Three *SLFN12*-targeting shRNAs were used, all of which were obtained from the TRC (CloneIDs: TRCN0000152141 and TRCN0000153520). Infected cells were selected using 1 μg/ml puromycin for 3 days and then grown in non-selective media for 3 more days. Cells were then plated into 384-well assay plates and tested for drug sensitivity as described above. Knockdown of *SLFN12* was validated by qPCR. Total RNA was extracted using the RNeasy Mini Kit (Qiagen #74104) and QIAschredder (Qiagen #79656). cDNA was generated using SuperScript III First-Strand Synthesis System (Life Technologies #18080-051). qPCR was performed for *GAPDH* and *SLFN12* (Life Technologies Hs00430118_m1) according to the manufacturers recommendations. *SLFN12* expression was normalized to corresponding samples *GAPDH* ct-values.

Supplementary Material

Refer to Web version on PubMed Central for supplementary material.

ACKNOWLEDGMENTS

This work was supported in part by National Cancer Institute Grant (grant number 1R35CA197568, awarded to M.M.), the American Cancer Society Research Professorship (awarded to M.M.), the Doctors Cancer Foundation (awarded to H.G.), the Friends of Dana-Farber Cancer Institute (awarded to H.G.), and the NIH's Molecular Libraries Program Center Network (MLPCN) (grant number 3U54HG005032-05S1, awarded to H.G., M.M., and S.L.S.). The cancer cell-line profiling studies were supported in part by the NCI's Cancer Target Discovery and Development (CTD2) Network (grant number U01CA176152, awarded to S.L.S.). We thank A. Bhatt, H. Gannon, J. Jung, T. Sharifnia and all members of the Meyerson lab for their advice and helpful discussions. S.L.S is an Investigator at the Howard Hughes Medical Institute.

COMPETING FINANCIAL INTERESTS

L.d.W., T.A.L., X.W., P.A.C., S.L.S., H.G. and M.M. receive research support from Bayer. M.M is a founder, consultant and equity holder in Foundation Medicine. L.d.W., T.A.L., L.G., B.M., H.G. and M.M. are inventors on patent WO 2014/164704 A2.

REFERENCES

1. Ferlay J, et al. Cancer incidence and mortality worldwide: sources, methods and major patterns in GLOBOCAN 2012. Int. J. Cancer. 2015; 136:E359–E386. [PubMed: 25220842]
2. Moffat JG, Rudolph J, Bailey D. Phenotypic screening in cancer drug discovery - past, present and future. Nat Rev Drug Discov. 2014; 13:588–602. [PubMed: 25033736]
3. Simons SS, Edwards DP, Kumar R. Minireview: dynamic structures of nuclear hormone receptors: new promises and challenges. Mol. Endocrinol. 2014; 28:173–182. [PubMed: 24284822]
4. Drake CG, Lipson EJ, Brahmer JR. Breathing new life into immunotherapy: review of melanoma, lung and kidney cancer. Nat Rev Clin Oncol. 2014; 11:24–37. [PubMed: 24247168]
5. Weinstein JN, et al. An information-intensive approach to the molecular pharmacology of cancer. Science. 1997; 275:343–349. [PubMed: 8994024]
6. Bredel M, Jacoby E. Chemogenomics: an emerging strategy for rapid target and drug discovery. Nat. Rev. Genet. 2004; 5:262–275. [PubMed: 15131650]
7. Weinstein JN, et al. Neural computing in cancer drug development: predicting mechanism of action. Science. 1992; 258:447–451. [PubMed: 1411538]
8. Barretina J, et al. The Cancer Cell Line Encyclopedia enables predictive modelling of anticancer drug sensitivity. Nature. 2012; 483:603–607. [PubMed: 22460905]
9. Basu A, et al. An interactive resource to identify cancer genetic and lineage dependencies targeted by small molecules. Cell. 2013; 154:1151–1161. [PubMed: 23993102]
10. Garnett MJ, et al. Systematic identification of genomic markers of drug sensitivity in cancer cells. Nature. 2012; 483:570–575. [PubMed: 22460902]
11. Staunton JE, et al. Chemosensitivity prediction by transcriptional profiling. Proc. Natl. Acad. Sci. U.S.A. 2001; 98:10787–10792. [PubMed: 11553813]
12. Zheng XFS, Chan T-F. Chemical genomics: a systematic approach in biological research and drug discovery. Curr Issues Mol Biol. 2002; 4:33–43. [PubMed: 11931568]
13. Crews CM. Targeting the undruggable proteome: the small molecules of my dreams. Chem. Biol. 2010; 17:551–555. [PubMed: 20609404]
14. Collins I, Workman P. New approaches to molecular cancer therapeutics. Nature Chemical Biology. 2006; 2:689–700. [PubMed: 17108987]
15. Swinney DC, Anthony J. How were new medicines discovered? Nat Rev Drug Discov. 2011; 10:507–519. [PubMed: 21701501]
16. Krönke J, et al. Lenalidomide causes selective degradation of IKZF1 and IKZF3 in multiple myeloma cells. Science. 2014; 343:301–305. [PubMed: 24292625]
17. Lu G, et al. The myeloma drug lenalidomide promotes the cereblon-dependent destruction of Ikaros proteins. Science. 2014; 343:305–309. [PubMed: 24292623]

18. Nakajima H, Kim YB, Terano H, Yoshida M, Horinouchi S. FR901228, a potent antitumor antibiotic, is a novel histone deacetylase inhibitor. Exp. Cell Res. 1998; 241:126–133. [PubMed: 9633520]
19. Marks PA, Breslow R. Dimethyl sulfoxide to vorinostat: development of this histone deacetylase inhibitor as an anticancer drug. Nat Biotechnol. 2007; 25:84–90. [PubMed: 17211407]
20. Ledermann J, et al. Olaparib maintenance therapy in patients with platinum-sensitive relapsed serous ovarian cancer: a preplanned retrospective analysis of outcomes by BRCA status in a randomised phase 2 trial. Lancet Oncol. 2014; 15:852–861. [PubMed: 24882434]
21. Lawrence MS, et al. Discovery and saturation analysis of cancer genes across 21 tumour types. Nature. 2014; 505:495–501. [PubMed: 24390350]
22. Francis SH, Blount MA, Corbin JD. Mammalian cyclic nucleotide phosphodiesterases: molecular mechanisms and physiological functions. Physiol. Rev. 2011; 91:651–690. [PubMed: 21527734]
23. Maurice DH, et al. Advances in targeting cyclic nucleotide phosphodiesterases. Nat Rev Drug Discov. 2014; 13:290–314. [PubMed: 24687066]
24. Tefferi A, Silverstein MN, Petitt RM, Mesa RA, Solberg LA. Anagrelide as a new platelet-lowering agent in essential thrombocythemia: mechanism of actin, efficacy, toxicity, current indications. Semin. Thromb. Hemost. 1997; 23:379–383. [PubMed: 9263355]
25. Burgin AB, et al. Design of phosphodiesterase 4D (PDE4D) allosteric modulators for enhancing cognition with improved safety. Nat Biotechnol. 2010; 28:63–70. [PubMed: 20037581]
26. Gurney ME, D'Amato EC, Burgin AB. Phosphodiesterase-4 (PDE4) molecular pharmacology and Alzheimer's disease. Neurotherapeutics. 2015; 12:49–56. [PubMed: 25371167]
27. Ruppert D, Weithmann KU. HL 725, an extremely potent inhibitor of platelet phosphodiesterase and induced platelet aggregation in vitro. Life Sci. 1982; 31:2037–2043. [PubMed: 6294426]
28. Cong L, et al. Multiplex genome engineering using CRISPR/Cas systems. Science. 2013; 339:819–823. [PubMed: 23287718]
29. Millar JK, et al. DISC1 and PDE4B are interacting genetic factors in schizophrenia that regulate cAMP signaling. Science. 2005; 310:1187–1191. [PubMed: 16293762]
30. Beca S, et al. Phosphodiesterase type 3A regulates basal myocardial contractility through interacting with sarcoplasmic reticulum calcium ATPase type 2a signaling complexes in mouse heart. Circ. Res. 2013; 112:289–297. [PubMed: 23168336]
31. Pozuelo Rubio M, Campbell DG, Morrice NA, Mackintosh C. Phosphodiesterase 3A binds to 14-3-3 proteins in response to PMA-induced phosphorylation of Ser428. Biochem. J. 2005; 392:163–172. [PubMed: 16153182]
32. Malovannaya A, et al. Analysis of the human endogenous coregulator complexome. Cell. 2011; 145:787–799. [PubMed: 21620140]
33. Chavez JA, Gridley S, Sano H, Lane WS, Lienhard GE. The 47kDa Akt substrate associates with phosphodiesterase 3B and regulates its level in adipocytes. Biochem. Biophys. Res. Commun. 2006; 342:1218–1222. [PubMed: 16516160]
34. Pierson E, et al. Sharing and Specificity of Co-expression Networks across 35 Human Tissues. PLoS Comput. Biol. 2015; 11:e1004220. [PubMed: 25970446]
35. Ahmad F, Degerman E, Manganiello V. Cyclic Nucleotide Phosphodiesterase 3 Signaling Complexes. Horm Metab Res. 2012; 44:776–785. [PubMed: 22692928]
36. Bedenis R, et al. Cilostazol for intermittent claudication. Cochrane Database Syst Rev. 2014; 10:CD003748. [PubMed: 25358850]
37. Movsesian M, Wever-Pinzon O, Vandeput F. PDE3 inhibition in dilated cardiomyopathy. Curr Opin Pharmacol. 2011; 11:707–713. [PubMed: 21962613]
38. Sun L, et al. Phosphodiesterase 3/4 inhibitor zardaverine exhibits potent and selective antitumor activity against hepatocellular carcinoma both in vitro and in vivo independently of phosphodiesterase inhibition. PLoS ONE. 2014; 9:e90627. [PubMed: 24598942]
39. Fryknäs M, et al. Phenotype-based screening of mechanistically annotated compounds in combination with gene expression and pathway analysis identifies candidate drug targets in a human squamous carcinoma cell model. J Biomol Screen. 2006; 11:457–468. [PubMed: 16928983]

40. Wang G, Franklin R, Hong Y, Erusalimsky JD. Comparison of the biological activities of anagrelide and its major metabolites in haematopoietic cell cultures. Br. J. Pharmacol. 2005; 146:324–332. [PubMed: 16041400]
41. Espasandin Y, et al. Anagrelide platelet-lowering effect is due to inhibition of both megakaryocyte maturation and proplatelet formation: insight into potential mechanisms. J. Thromb. Haemost. 2015:n/a–n/a.
42. Card GL, et al. Structural basis for the activity of drugs that inhibit phosphodiesterases. Structure. 2004; 12:2233–2247. [PubMed: 15576036]
43. Zhang W, Ke H, Colman RW. Identification of interaction sites of cyclic nucleotide phosphodiesterase type 3A with milrinone and cilostazol using molecular modeling and site-directed mutagenesis. Mol. Pharmacol. 2002; 62:514–520. [PubMed: 12181427]
44. Lee ME, Markowitz J, Lee JO, Lee H. Crystal structure of phosphodiesterase 4D and inhibitor complex(1). FEBS Lett. 2002; 530:53–58. [PubMed: 12387865]
45. Nagao M, et al. Role of protein phosphatases in malignant transformation. Int. Symp. Princess Takamatsu Cancer Res. Fund. 1989; 20:177–184. [PubMed: 2562181]
46. Imielinski M, et al. Mapping the hallmarks of lung adenocarcinoma with massively parallel sequencing. Cell. 2012; 150:1107–1120. [PubMed: 22980975]
47. Lawrence MS, et al. Mutational heterogeneity in cancer and the search for new cancer-associated genes. Nature. 2013; 499:214–218. [PubMed: 23770567]
48. Kaheinen P, et al. Positive inotropic effect of levosimendan is correlated to its stereoselective Ca2+-sensitizing effect but not to stereoselective phosphodiesterase inhibition. Basic Clin. Pharmacol. Toxicol. 2006; 98:74–78. [PubMed: 16433895]
49. Tang KM, Jang EK, Haslam RJ. Photoaffinity labelling of cyclic GMP-inhibited phosphodiesterase (PDE III) in human and rat platelets and rat tissues: effects of phosphodiesterase inhibitors. European Journal of Pharmacology. 1994; 268:105–114. [PubMed: 7925608]
50. Altman DG, Bland JM. Measurement in Medicine: The Analysis of Method Comparison Studies. The Statistician. 1983; 32:307.

REFERENCES

51. Rappsilber J, Mann M, Ishihama Y. Protocol for micro-purification, enrichment, pre-fractionation and storage of peptides for proteomics using StageTips. Nat Protoc. 2007; 2:1896–1906. [PubMed: 17703201]
52. Udeshi ND, et al. Methods for Quantification of in vivo Changes in Protein Ubiquitination following Proteasome and Deubiquitinase Inhibition. Mol Cell Proteomics. 2012; 11:148–159. [PubMed: 22505724]

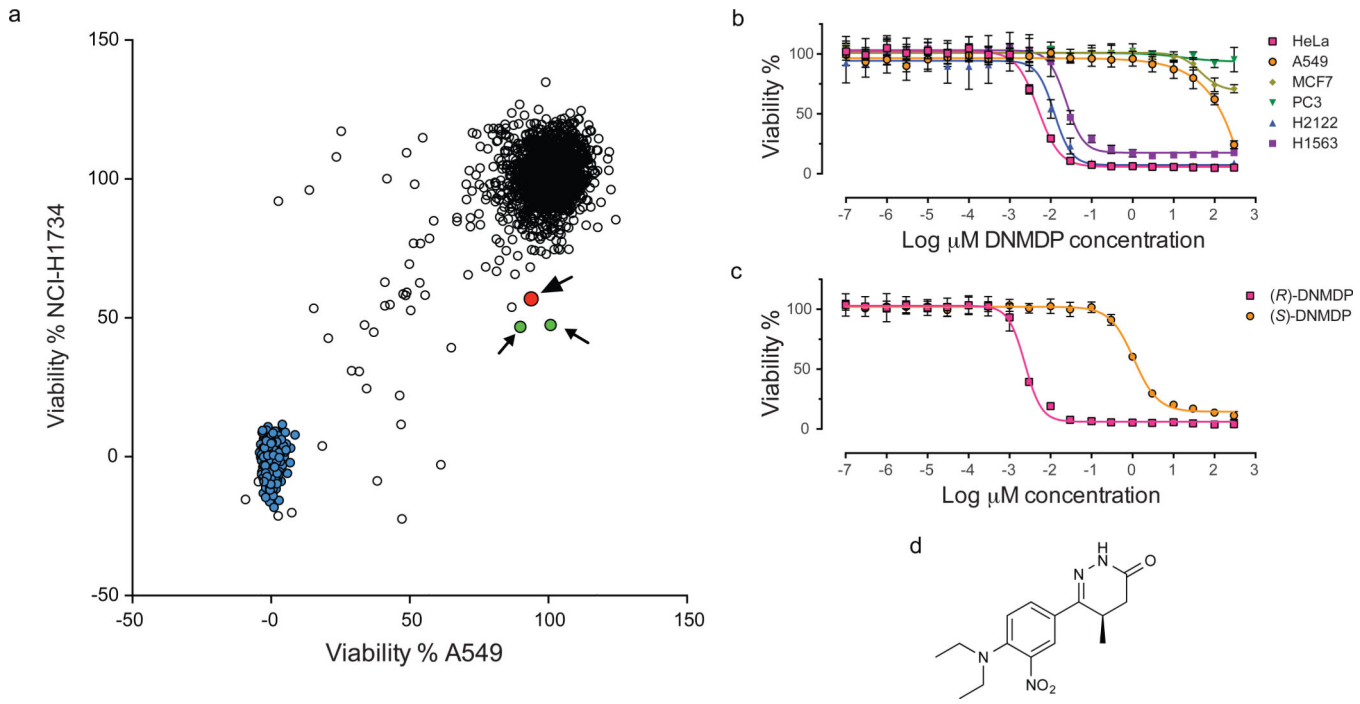

Figure 1. Identification and characterization of DNMDP, a potent and selective cancer cell cytotoxic agent

(**a**) Scatterplot of 1924 compounds shows mean survival of *TP53* mutant NCI-H1734 cells and *TP53* wild-type A549 cells after 48 hours of treatment at concentrations of 10 μM. DNMDP is indicated in red with an arrow. Other compounds that selectively killed NCI-H1734 cells are indicated in green with a small arrow. Positive control staurosporine is labeled in blue. (**b**) A panel of cell lines was treated with the indicated concentrations of DNMDP for 48 hours. Data represent mean values of 8 replicates ± s.d. (**c**) The HeLa cell line was treated with indicated concentrations of the separated enantiomers of DNMDP for 48 hours. The (*R*)-enantiomer had a 500-fold lower EC_{50} compared to the (*S*)-enantiomer. Data represent mean values of 8 replicates ± s.d (**d**) Structure of (*R*)-DNMDP.

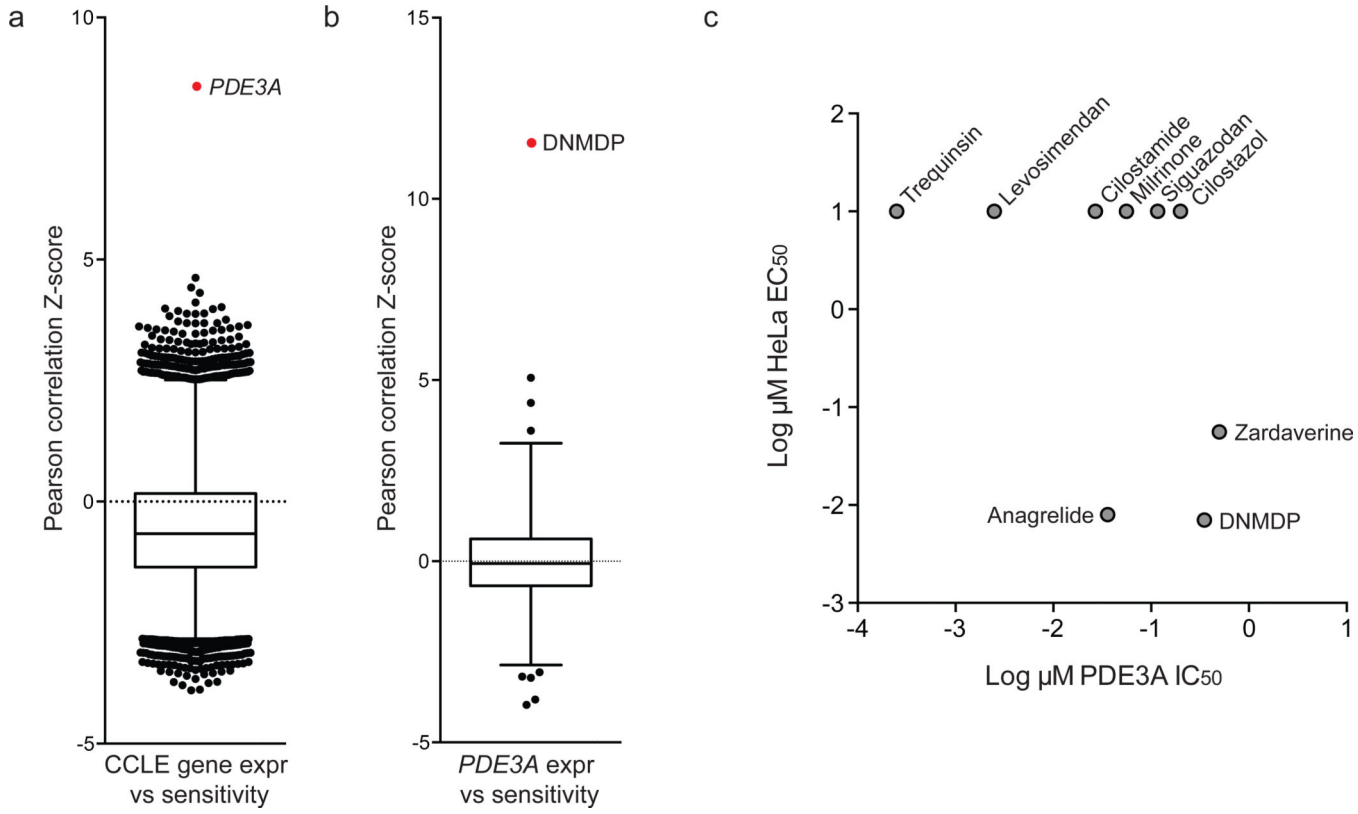

Figure 2. *PDE3A* expression correlates with sensitivity to DNMDP, but inhibition of PDE3A mediated cAMP hydrolysis does not correlate with cytotoxicity

(**a**) Correlation between DNMDP sensitivity and expression of 18,988 genes in 766 genomically characterized cell lines. Cell lines were treated for 72 hours with concentrations ranging from 66.4 µM – 2 nM in 2-fold step dilutions. The Z-score for Pearson correlation between *PDE3A* expression and sensitivity to DNMDP is 8.5. (**b**) Cell lines from panel A were treated with 480 compounds. DNMDP shows the best correlation between *PDE3A* expression and sensitivity. (**c**) Published PDE3 inhibitor IC_{50} values and EC_{50} values of HeLa treated with indicated compounds up to 10 µM for 48 hours[23,27,48,49]. DNMDP IC_{50} concentration for PDE3A inhibition was determined in Supplementary Fig. 5b.

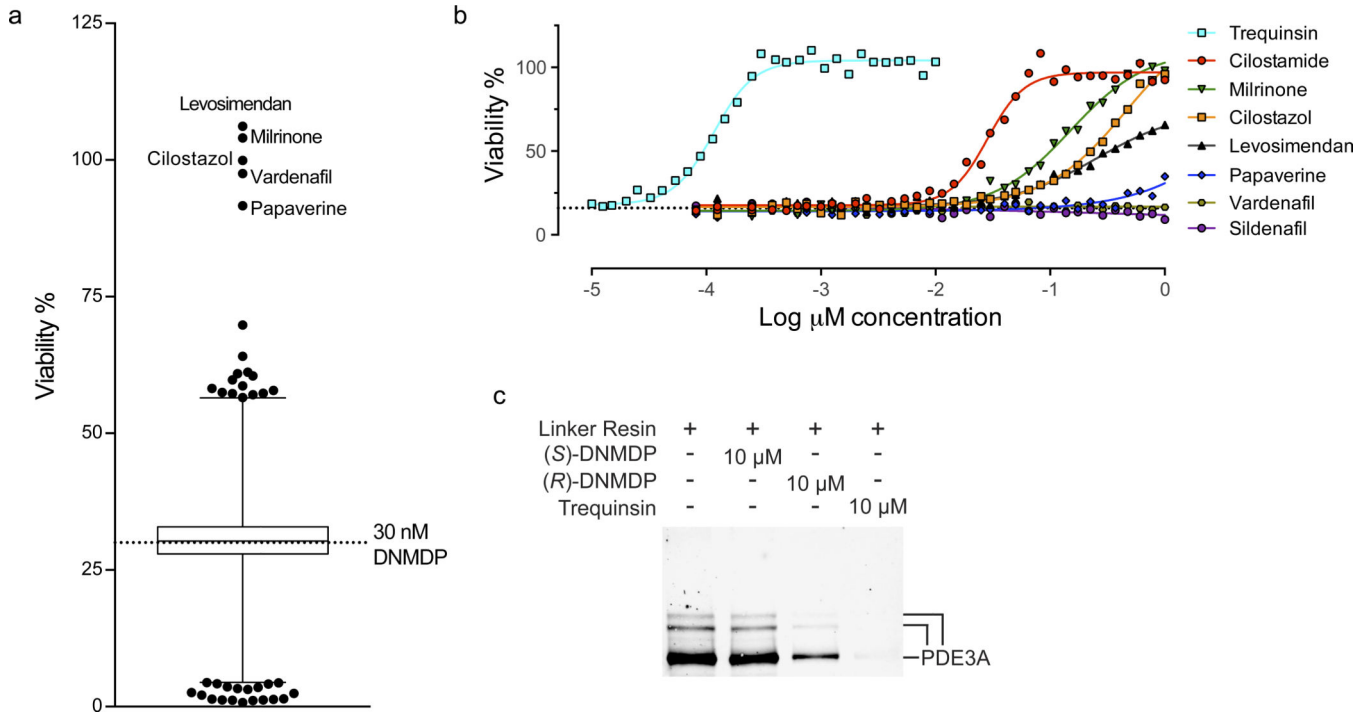

Figure 3. Non-lethal PDE3 inhibitors rescue cell death induced by DNMDP by competing for the binding of PDE3A

(**a**) HeLa cells were treated with 1600 bioactive compounds at a concentration of 20 μM in combination with 30 nM (EC_{70}) of DNMDP for 48 hours. The viability was calculated as a percentage of the untreated DMSO control. (**b**) HeLa cells were treated with DNMDP in combination with indicated concentrations of non-lethal PDE3 and pan-PDE inhibitors for 48 hours. Data represent values of single data points. (**c**) Affinity purification performed on 200 μg of HeLa cell lysate using a DNMDP linker-analogue tethered to a solid phase with the same rescue characteristic as non-lethal PDE3 inhibitors. Indicated compounds were co-incubated with the linker-analogue. The affinity purified fraction was run on an SDS-PAGE gel and probed for PDE3A.

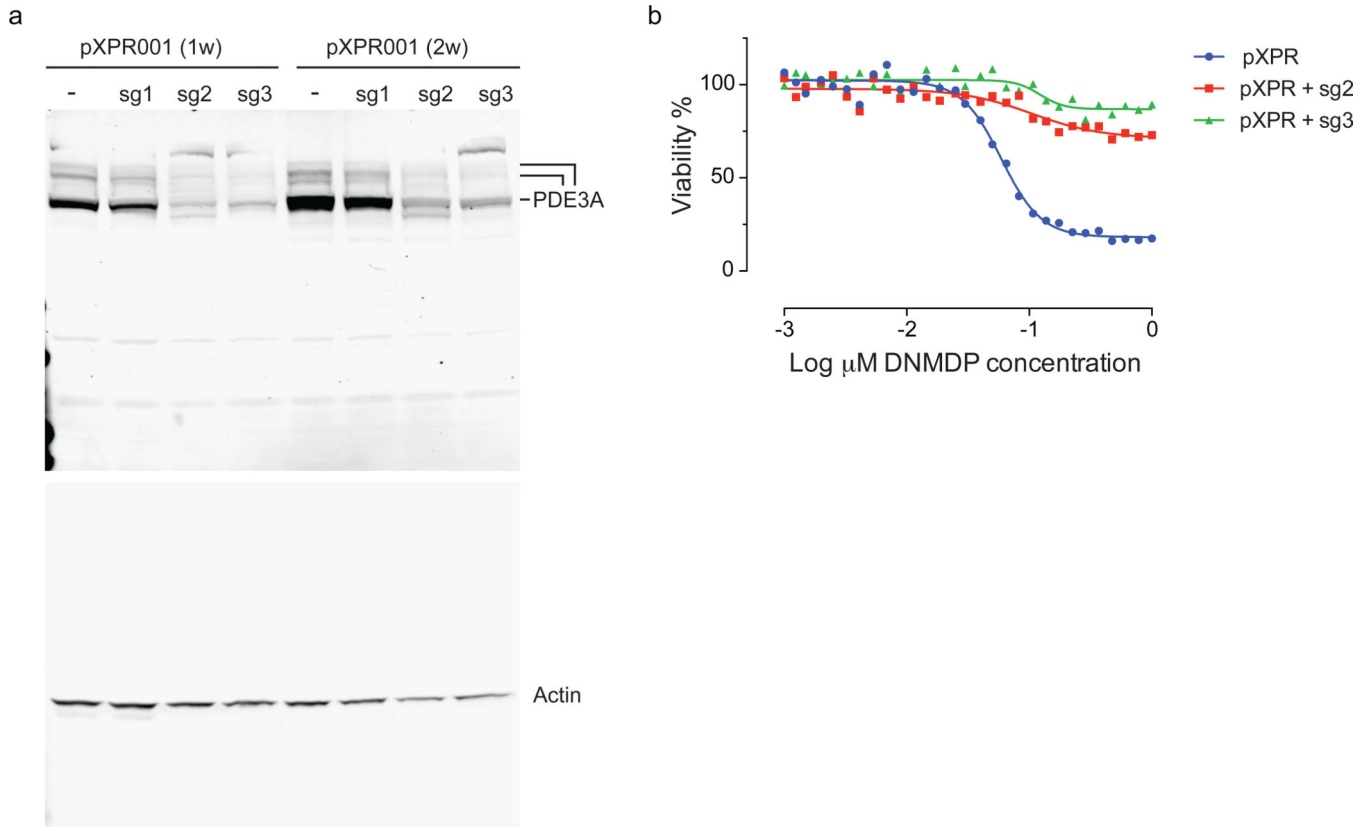

Figure 4. PDE3A is not essential in sensitive cell lines but is required for relaying the cytotoxic signal

(**a**) HeLa cells were infected with Cas9 and indicated guide RNAs (SG) against *PDE3A*. Western blots were probed for PDE3A at indicated time points. (**b**) HeLa cells were infected with indicated sgRNAs for two weeks and treated with 1 μM of DNMDP for 48 hours. Percent rescue was normalized to the Cas9-only control. Data represent values of single data points

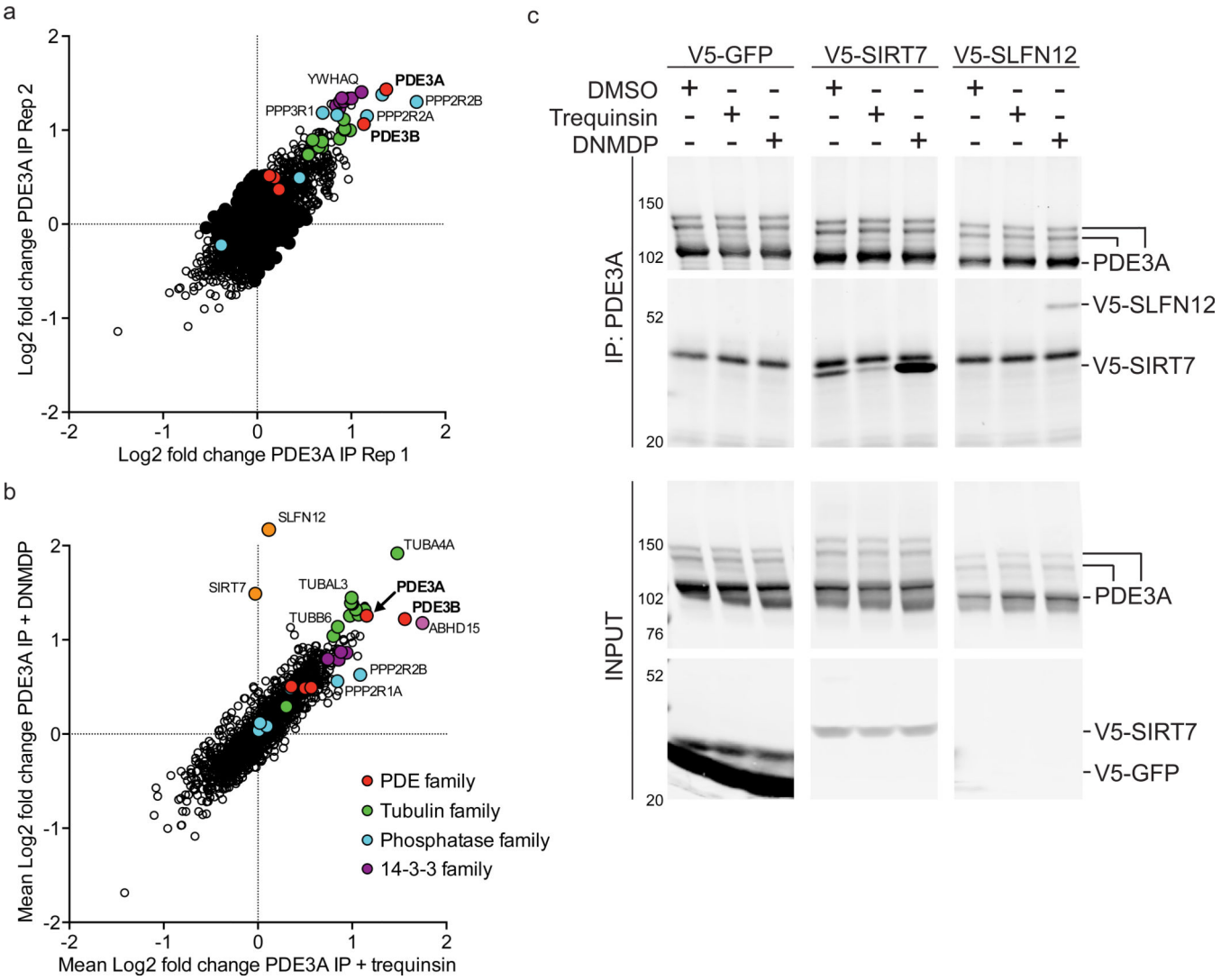

Figure 5. PDE3A immunoprecipitation in the presence of DNMDP reveals novel SIRT7 and SLFN12 interaction

(**a**) The scatter plot shows $\log_2$ ratios for proteins that were enriched in anti-PDE3A immunoprecipitates in the DMSO treated HeLa cells compared to anti-PDE3A immunoprecipitates in the presence of blocking peptide specific to the PDE3A antibody; each dot represents a protein. (**b**) Log_2 ratios of changes of proteins bound to PDE3A in the presence of DNMDP *versus* trequensin. Each dot represents the average of two replicates per condition for an individual protein. In all cases, the data plotted passed the Bland-Altman test with 95% confidence interval for reproducibility[50]. (**c**) HeLa cells were transfected with indicated plasmids and treated with indicated compounds with a final concentration of 10 μM for four hours. Endogenous PDE3A was immunoprecipitated and immunoblotted for V5 to identify novel interaction with SIRT7 and SLFN12 (upper two panels). Immunoprecipitate input was immunoblotted for PDE3A and V5 (lower two panels). V5-SLFN12 was undetectable in whole cell lysate.

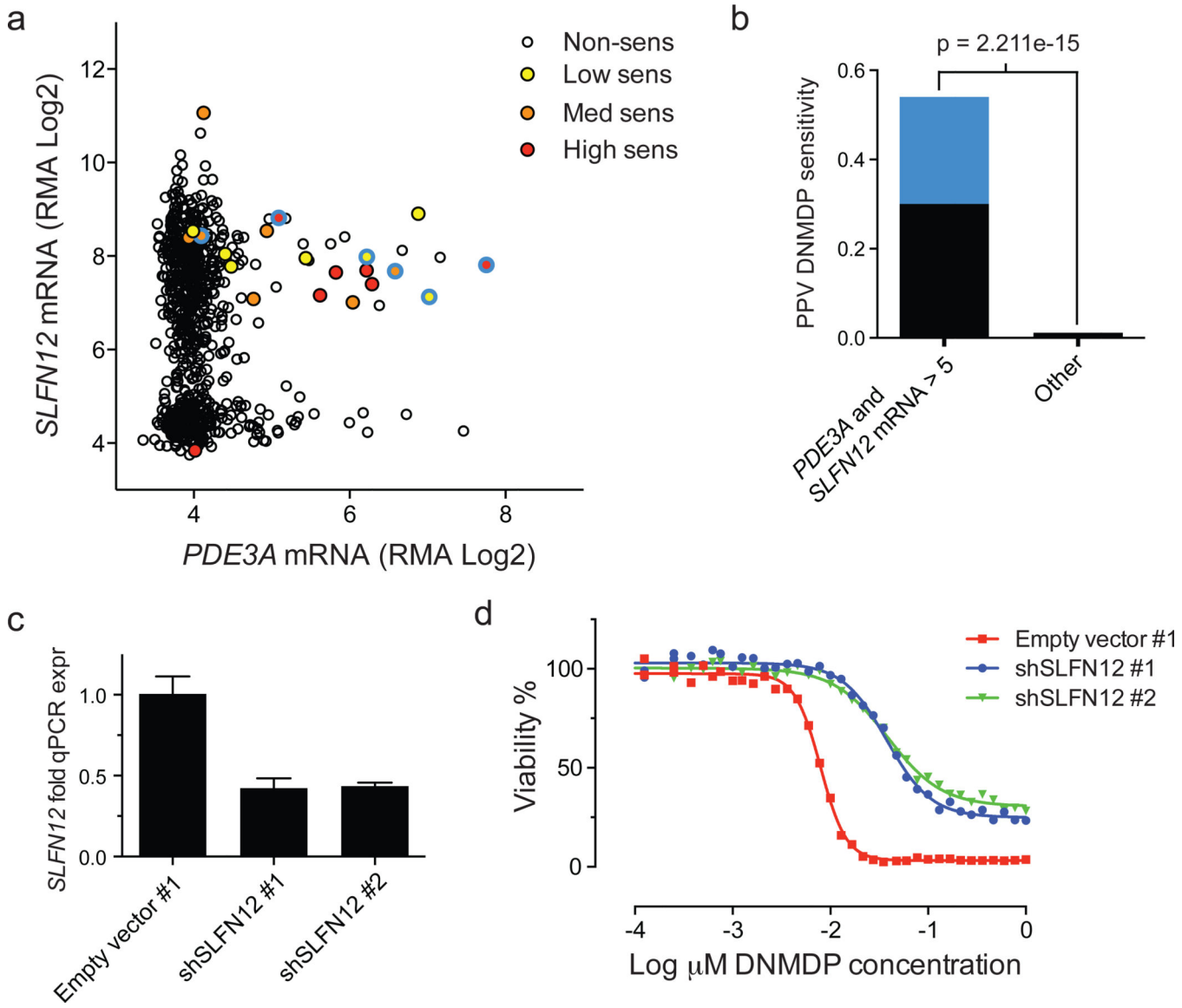

Figure 6. Cell lines with dual expression of *SLFN12* and *PDE3A* are significantly enriched for DNMDP-sensitive cell lines

(**a**) mRNA RMA expression values for *PDE3A* and *SLFN12* from the CCLE database with sensitive cell lines indicated[8]. 21 sensitive cell lines were binned in three groups of 7 based on AUC rank. (**b**) Fisher's exact test on DNMDP sensitivity of cell lines with high expression of both *SLFN12* and *PDE3A* (RMA Log2 > 5) compared to other cell lines. Light blue indicates melanoma cell lines. (**c**) qPCR expression changes of *SLFN12* in HeLa cells transduced with shSLFN12 normalized to GAPDH. (**d**) HeLa cells were transduced with indicated shRNA reagents and treated with indicated concentrations of DNMDP for 72 hours. Data represent values of single data points.